Heat transfer and entropy generation of water–Fe$_3$O$_4$ nanofluid under magnetic field by Euler–Lagrange method

Arash Rezaei Gorjaei[1] · Fatemeh Joda[1] · Ramin Haghighi Khoshkhoo[1]

Abstract

The Euler–Lagrange method is considered to simulate the water–Fe$_3$O$_4$ nanofluid inside a circular tube. The non-uniform magnetic field is employed to a part of the tube. The effects of Reynolds number, concentration and magnetic field are investigated. The obtained results show that by increasing the magnetic field strength, global frictional entropy generation rate enhances. Meanwhile, with the application of the magnetic field, the frictional entropy generation rate in the central region of the tube and the vicinity of the wall decreases and increases, respectively. Additionally, the Bejan number is approximately 1 near the outlet. Also, there is a non-uniform distribution for nanoparticles, and the concentration of nanoparticles in the tube center is higher than the wall adjacency. Moreover, the wall temperature of the tube decreases in the part where the magnetic field is applied. The use of nanoparticle leads to an increase in the convective heat transfer coefficient. The velocity of the nanofluid in the central part of the tube decreases with the application of the magnetic field. But, the flow velocity near the wall increases with increasing magnetic field strength.

Keywords Nanofluid · Concentration · Entropy generation · Magnetic field · Euler–Lagrange

List of symbols

Be	Bejan number
C_c	Cunningham correction factor
C_s	Constant
C_t	Constant
C_m	Constant
C_p	Specific heat (J kg^{-1} K^{-1})
d_p	Nanoparticle diameter (nm)
d_{ij}	Deformation tensor (s^{-1})
F	Total force per unit mass (N kg^{-1})
F_B	Brownian force (N kg^{-1})
F_D	Drag force (N kg^{-1})
F_L	Saffman lift force (N kg^{-1})
F_M	Magnetic force (N kg^{-1})
F_T	Thermophoretic force (N kg^{-1})
H	Magnetic field strength (A m^{-1})
h	Convective heat transfer coefficient (W m^{-2} K^{-1})
k	Thermal conductivity (W m^{-1} K^{-1})
k_B	Boltzmann constant (J K^{-1})
Kn	Knudsen number
k_s	Coefficient
L	Length of the tube (m)
M	Magnetization
m	Magnetic moment (Am^2)
m_p	Particle mass (kg)
n_p	Number of solid particles within a cell volume
p	Pressure (Pa)
ΔP	Pressure drop (Pa)
Pr	Prandtl number
q''	Heat flux (W m^{-2})
Re	Reynolds number
Re_p	Reynolds number of the particle
r	Radius of the tube (m)
S_0	Spectral intensity basis
S_{nij}	Spectral intensity
S_{Pe}	Energy source term (kg m^{-1} s^{-3})
S_{Pm}	Momentum source term (kg m^{-2}s^{-2})
$\dot{S}'''_{g,f}$	Frictional entropy generation rate (W m^{-3} K^{-1})
$\dot{S}'''_{g,h}$	Thermal entropy generation rate (W m^3 K^{-1})
$\dot{S}'''_{g,t}$	Total entropy generation rate (W m^{-3} K^{-1})
T	Temperature (K)
t	Time (s)
V	Velocity (m s^{-1})
$\forall$	Volume (m^3)

✉ Fatemeh Joda
  f_joda@sbu.ac.ir

[1] Faculty of Mechanical and Energy Engineering, Shahid Beheshti University, Tehran, Iran

$\delta\forall$ Cell volume (m^3)
X Dimensionless parameter
x Axial direction
y Radial direction

Greek letters

δ_{ij} Kronecker delta function
λ Molecular mean free path (m)
μ Dynamic viscosity (Ns m^{-2})
μ_B Bohr magneton (Am^2)
μ_0 Magnetic permeability (Tm A^{-1})
v Kinematic viscosity (m^2 s^{-1})
ξ Argument of Langevin function
ξ_i Unit-variance-independent Gaussian random number
ρ Density (kg m^{-3})
ϕ Concentration (%)

Subscripts

b Bulk
f Fluid
in Inlet
p Particle
w Wall

Introduction

One of the most important problems in the twenty-first century and following centuries is energy savings. So, many researchers have made important studies on this topic. Improving the useful life of equipment and saving the energy can be achieved by increasing heating (or cooling) in thermal devices. So far, many methods have been proposed by various researchers to save energy.

Due to the remarkable properties of nanofluids, especially their extreme thermal conductivity, many research studies have been carried out in the nanofluids field [1–17]. Recently, nanofluids have been widely used in the petro-chemical industry, nanomedicine and consumer products. One of the many considerations is the use of nanofluids to increase convection heat transfer. Therefore, the process of cooling and heating in the equipment is carried out more quickly.

One of the most modern collections of nanofluids is magnetic nanofluids. This type of nanofluids, in addition to having good thermal transfer properties, can response and react to the magnetic field. Nowadays, these branches of the nanofluids have been widely used in medicine and the industry. In recent years, a number of researchers have used ferrofluids to examine heat transfer [18–23]. Esmaeili et al. [24] examined heat transfer in a magnetic nanofluid within copper pipe with a length of 1.2 m and an internal diameter of 6.8 mm. The effect of the magnetic field has been studied in their work. It has been shown that by varying the frequency of the magnetic field from 50 Hz to 1 MHz, the heat transfer of water-based nanofluid increased by 48%. While using ethylene glycol as a base fluid in the same conditions, the amount of heat transfer increased by 15%. Bahiraei and Hangi [25] simulated the flow behavior of magnetic nanofluid in a heat exchanger. In their work, the effect of volume fraction, nanoparticle size and magnetic field on nanofluid flow and heat transfer properties has been considered. They showed that the larger diameter of the nanoparticles leads to enhance the heat transfer. It should also be noted that they showed that the pressure drop also increased with increasing diameter of the nanoparticles. By increasing the nanoparticles' volume fraction, the hot fluid temperature will decrease over the heat exchanger. Also, with increasing magnetic field, the overall heat transfer coefficient increases. Sheikhnejad et al. [26] studied the flow of ferrofluid under a magnetic field effect as a way to increase heat transfer inside a pipe. The constant heat flux was applied as a thermal boundary condition for the test section. The use of magnetic field and nanoparticles results in a higher Darcy friction coefficient. Yarahmadi et al. [27] examined forced convection through a magnetic nanofluid at constant and oscillating magnetic fields. Their experimental work has been conducted in a pipe with boundary conditions of constant heat flux and a laminar flow regime. In their work, the effects of Reynolds number, volume fraction, intensity and arrangement of magnetic field on the heat transfer have been studied.

To simulate the nanofluids flow, single-phase and two-phase methods can be used [28–31]. Since several factors such as Brownian force, thermophoretic force, friction between base fluid and nanoparticles, gravity and dispersion may occur in nanofluids, some researchers have tried to achieve more realistic results using two-phase methods for nanofluids. So far, two-phase models have been proposed including the Euler–Euler model and the Euler–Lagrange model.

The irreversible factors can be minimized by applying the second law of thermodynamics. Therefore, in the study of nanofluids flow, in addition to the first law of thermodynamics, it is necessary to consider the second law of thermodynamics, which can be a criterion for the operation of engineering devices. In recent years, some researchers have exerted entropy generation to investigate the behavior of fluids [32–38]. Mahmud and Fraser [39] analytically investigated entropy generation in a non-Newtonian fluid flow. They reported that with the increase of the power law index, the entropy generation rate would increase. Bahiraei et al. [40] studied the behavior of nanofluid flow containing graphene nanoparticles by considering entropy

generation and exergy destruction. Their studied geometry was a micro-heat exchanger. In their simulation, the viscous dissipation was considered. They showed that the addition of nanoparticles leads to increased frictional and thermal exergy destruction. Shahsavar et al. [41] calculated the entropy generation in a magnetic nanofluid flow within a micro-channel. Their geometry was under magnetic field. In their work, it has been shown that the frictional entropy generation rate increases with increasing magnetic field intensity, while thermal entropy generation rate decreases. Rezaei Gorjaei et al. [42] investigated entropy generation and heat transfer in water–Al₂O₃ nanofluid. Two-phase mixture method was used to simulate nanofluid. In their work, the Bejan number, the frictional and thermal entropy generation rates were calculated. Simulation results show that entropy generation and heat transfer increase with increasing nanofluid concentration. It is also shown that Bejan number is close to 1.

The present simulation considers the second law of thermodynamics (thermal and frictional entropy generation rate) in the water–Fe₃O₄ nanofluid. Moreover, in the current simulation, the effects of Reynolds number, concentration and magnetic field strength are evaluated on the convective heat transfer coefficient, pressure drop and nanoparticles distribution. The non-uniform magnetic field is employed to a part of the tube. The magnetic field strength is linear, and it has a negative gradient. To simulate the nanofluid, the Euler–Lagrange method is applied. However, in most of the previous studies, single-phase and Euler–Euler methods have been used to study nanofluid behavior.

Geometry and magnetic field

The studied heat exchanger is a tube, which is simulated in two-dimensional mode. The fluid used inside the tube is water–Fe₃O₄ nanofluid. The length of the tube is 130 times the radius of the tube ($L = 130\ r$). Figure 1 shows schematic of the geometry. The non-uniform magnetic field is applied on a part of tube (from $X = x/L = 0.3$ to $X = 0.61$), and the constant heat flux is applied on the tube wall. The magnetic field has a negative gradient, and the magnetic
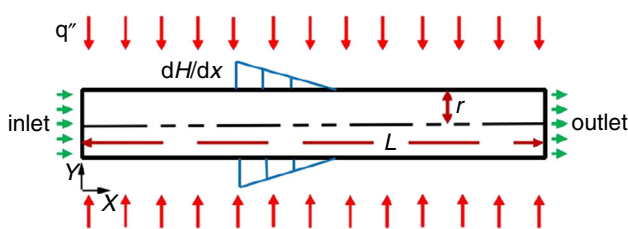
field strength (H) decreases linearly. That is, at the point $X = 0.3$, it has the maximum value, and at $X = 0.61$ it reaches its lowest value. At the tube outlet, a zero relative pressure is applied. At the tube inlet, uniform temperature and velocity are applied for continuous phase and nanoparticles.

Euler–Lagrange method

The evaluation of the characteristics of the nanofluid flow (water–Fe₃O₄) that flows inside the tube is carried out using the Euler–Lagrange method. In this method, only the properties of the water and nanoparticles are needed and do not depend on effective models for calculating thermophysical properties. Also, the fluid is applied as a continuous phase with the nanoparticles dispersed inside it. Therefore, the governing equations are as follows:

Continuity equation

$$\nabla \cdot (\rho_f V_f) = 0 \tag{1}$$

Momentum equation

$$\nabla \cdot (\rho_f V_f V_f) = -\nabla P + \nabla \cdot (\mu_f \nabla V_f) + S_{p,m} \tag{2}$$

Energy equation

$$\nabla \cdot (\rho_f C_{p,f} V_f T_f) = \nabla \cdot (k_f \nabla T_f) + S_{p,e} \tag{3}$$

where P and T indicate pressure and temperature, respectively. Also, k, ρ, μ and C_p are thermal conductivity, density, dynamic viscosity and the specific heat. The subscript f refers to the continuous phase. The source terms of $S_{p,m}$ and $S_{p,e}$ are defined as below [43]:

$$S_{p,m} = \sum n_p \frac{m_p}{\delta \forall} F \tag{4}$$

$$S_{p,e} = \sum n_p \frac{m_p}{\delta \forall} C_p \frac{dT_p}{dt} \tag{5}$$

where F and m_p, respectively, represent total force per unit mass of the particle acting on it and particle mass, n_p is the number of solid particles within a cell volume, and $\delta \forall$ represents the cell volume. Also, subscript p refers to nanoparticle.

In Eq. (4), the parameter F is comprised of different forces including magnetic force, Brownian force, Saffman lift force, drag force and thermophoretic force.

$$F = F_D + F_L + F_T + F_B + F_M. \tag{6}$$

Gravity is neglected, because it is not significant compared with other forces [44].

The drag force (F_D) is obtained by various formulas. A form of Stokes' drag law is employed for submicron particles [45].

Fig. 1 Schematic of studied geometry

$$F_D = \frac{18\mu_f}{d_p^2 \rho_p C_c}(V_f - V_p) \tag{7}$$

where C_c is Cunningham correction factor.

$$C_c = 1 + \frac{2\lambda}{d_p}\left(1.257 + 0.4e^{-(1.1d_p/2\lambda)}\right) \tag{8}$$

where d_p and λ represent the particle diameter and the molecular mean free path, respectively.

The Saffman lift force (F_L) [46]:

$$F_L = \frac{2 \times K_s \times v^{0.5}\rho_f d_{ij}}{\rho_p d_p (d_{ij}d_{ij})^{0.25}}(V_f - V_p) \tag{9}$$

where $K_s = 2.594$ and d_{ij} is the deformation tensor.

The thermophoretic force (F_T) [47]:

$$F_T = \frac{-6\pi\mu_f^2 d_p C_s}{\rho_f(1 + 3C_m Kn)}\frac{k_f/k_p + C_t Kn}{1 + 2(k_f/k_p) + 2C_t Kn}\frac{\nabla T}{m_p T} \tag{10}$$

where $C_m = 1.14$, $C_t = 2.18$ and $C_s = 1.17$.

The Brownian force ($F_{B,i}$):

$$F_{Bi} = \xi_i \left(\frac{\pi S_0}{\Delta t}\right)^{0.5} \tag{11}$$

where ξ_i denotes the unit-variance-independent Gaussian random number with zero mean. Different components of the Brownian force (F_B) are modeled as a Gaussian white noise process, while the spectral intensity of $S_{n,ij}$ is given by Li and Ahmadi [48]:

$$S_{n,ij} = S_0 \delta_{ij} \tag{12}$$

where δ_{ij} is the Kronecker delta function, and:

$$S_0 = \frac{216 v k_B T}{\pi^2 \rho_f d_p^5 \left(\frac{\rho_p}{\rho_f}\right)^2 C_c} \tag{13}$$

where k_B represents Boltzmann constant and v is the kinematic viscosity.

The magnetic force applied on the magnetic nanofluid is calculated by [49]:

$$F_{M,tot} = \mu_0 (M \cdot \nabla)H \tag{14}$$

where H denotes the magnetic field strength, M is magnetization, and μ_0 represents the magnetic permeability [50]:

$$M = N m L(\xi) = Nm\left(\coth \xi - \frac{1}{\xi}\right) \tag{15}$$

where ξ. is the Langevin function argument (L), N denotes the nanoparticles number in unit volume, and m represents the magnetic moment.

$$\xi = \frac{\mu_0 m H}{k_B T} \tag{16}$$

The force applied on a single magnetic particle in unit mass is calculated by:

$$F_M = \frac{\mu_0 m L(\xi)\nabla H}{m_p} \tag{17}$$

The magnetic moment of a nanoparticle is obtained by:

$$m = \frac{8 \times 4\mu_B \forall_p}{7.3 \times 10^{-28}} \tag{18}$$

where μ_B is Bohr magneton, and $\forall_p$ is volume.

Energy equation for nanoparticles is calculated by:

$$m_p C_{p,p}\frac{dT_p}{dt} = Nu_p \pi d_p k_f(T_f - T_p) \tag{19}$$

where Nu_p number is calculated by Eq. (20) (Ranz and Marshall [51]).

$$Nu_p = 2 + 0.6 Re_p^{0.5} Pr^{0.3} \tag{20}$$

where Pr is the Prandtl number, and Re_p represents the particle Reynolds number.

Data reduction

The total entropy generation rate is calculated by:

$$\dot{S}_{g,t}''' = \dot{S}_{g,h}''' + \dot{S}_{g,f}''' \tag{21}$$

where $\dot{S}_{g,h}'''$ and $\dot{S}_{g,f}'''$ are thermal and frictional entropy generation rates, respectively.

$$\dot{S}_{g,h}''' = \frac{k}{T^2}\left[\left(\frac{\partial T}{\partial x}\right)^2 + \left(\frac{\partial T}{\partial y}\right)^2\right] \tag{22}$$

$$\dot{S}_{g,f}''' = \frac{\mu}{T}\left\{2\left[\left(\frac{\partial u}{\partial x}\right)^2 + \left(\frac{\partial v}{\partial y}\right)^2\right] + \left(\frac{\partial u}{\partial y} + \frac{\partial v}{\partial x}\right)^2\right\} \tag{23}$$

With integration of local entropy generation rate, global entropy generation rate is obtained.

$$\dot{S}_{g,h} = \int \dot{S}_{g,h}''' d\forall \quad \text{and} \quad \dot{S}_{g,f} = \int \dot{S}_{g,f}''' d\forall \tag{24}$$

$$\dot{S}_{g,t} = \int \dot{S}_{g,t}''' d\forall = \int \dot{S}_{g,f}''' d\forall + \int \dot{S}_{g,h}''' d\forall \tag{25}$$

The Bejan number is the ratio of thermal entropy generation rate to total entropy generation rate and is calculated by:

$$Be = \frac{\dot{S}_{g,h}}{\dot{S}_{g,t}} \tag{26}$$

The convective heat transfer coefficient is obtained by:

$$h = \frac{q''}{T_w - T_b} \tag{27}$$

Numerical method

The simulation of the magnetic nanofluid flow in the tube is performed only on one side of the tube. Therefore, the governing equations are solved two-dimensionally. The finite volume procedure is used for solving the governing equations. The meshes are selected very finer near the tube wall, because the temperature and velocity gradients are severe near the tube wall. In fact, a non-uniform network is considered. For investigation of the mesh independence, a number of different meshes are analyzed, and finally, the 400*30 mesh are selected in the longitudinal and radial directions of geometry, respectively ($Re = 500$, $\phi = 0.03$, $d_\mathrm{p} = 50$ nm and $\frac{\mathrm{d}H}{\mathrm{d}x} = 0$). The mesh used in the present simulation is shown in Fig. 2. The errors presented for the average convective heat transfer coefficient are obtained with respect to the best grid results (see Table 1)

The accuracy of the simulation results of the Euler–Lagrange approach is compared with the data obtained from the experimental work of Kim et al. [52]. In their work, the nanofluid was carried out inside a tube at $\phi = 0.03$ and $Re = 1460$. Figure 3 shows the acceptable results for the current paper. The comparison parameter between the two studies is convective heat transfer coefficient. It is found that the maximum error is 5%; therefore, the present results are correct.

Results and discussion

The simulation of water–Fe₃O₄ nanofluid flow in this paper is carried out using the Euler–Lagrange method. The tube is investigated under a non-uniform magnetic field with different negative gradients. Also, different Reynolds numbers and three concentrations (ϕ) at $d_\mathrm{p} = 50$ nm (diameter of nanoparticles) are considered to evaluate the performance of the tube. In this research, the entropy generation (locally and globally), convective heat transfer coefficient, pressure drop, and distribution of nanoparticles concentration are studied.

In Fig. 4, the distribution of concentration of Fe₃O₄ nanoparticles at $\phi = 0.03$ and $Re = 500$ with and without magnetic field is shown in a cross section of the tube. As can be seen from this figure, there is a non-uniform distribution in the tube cross section for nanoparticles, and the
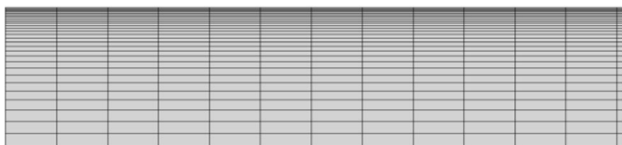
concentration of nanoparticles in the tube center is higher than the wall adjacency, which is generally attributed to the migration of Fe₃O₄ nanoparticles due to reasons like shear rate. In some papers, similar results have been reported for the non-uniform distribution of nanoparticles [53, 54]. However, most studies on nanofluid have used a single-phase method to simulate nanofluid, which, in their articles, it is assumed that the distribution of concentration is uniform [55, 56]. Moreover, this figure shows that in the presence of magnetic field, the distribution of concentration becomes more uniform. This is because the force of magnetic attracts the Fe₃O₄ nanoparticles toward the tube wall, and therefore, the nanoparticles concentration is enhanced near the wall.

If the magnetic field is applied, the velocity profile may change due to the distribution of nanoparticles non-uniform. In other words, because of the higher number of particles in the tube center (due to more concentration), the force in these regions becomes more important. For a cross section of tube at $\phi = 0.03$ and $Re = 500$, the velocity profile for different magnetic fields with negative gradients is shown in Fig. 5 (where subscript s refers to a magnetic field strength at $\phi = 0.03$ and $Re = 500$). In this figure, it can be seen that the velocity of the nanofluid in the central part of the tube decreases with the application of the magnetic field and the increase in its gradient. However, the nanofluid velocity near the wall increases with increasing magnetic field gradient. Because the gradient of the magnetic field is negative, the force exerted on the Fe₃O₄ nanoparticles is in the opposite direction of the nanofluid; due to the non-uniform concentration distribution in the cross section of the tube, the velocity increases near the tube wall and reduces in the central regions.

Figure 6 demonstrates the non-dimensional nanofluid velocity profile at a cross section for the concentration of 0.01, 0.03 and 0.05 (dH/dx = 0 and $Re = 500$). By approaching the tube central part, the velocity gradient decreases. It is found that the nanofluid flow at $\phi = 0.03$ and 0.05 possesses a flatter velocity profile in comparison with $\phi = 0.01$.

As shown in Fig. 7, the frictional entropy generation rate near the wall of the tube is highest, and in the central part, frictional entropy generation rates are very low ($\phi = 0.03$ and $Re = 500$). The changes obtained for the frictional entropy generation rate are due to the velocity gradient at the cross section of the tube. (As the tube wall is narrowed, the velocity profile changes slowly.) It can be seen from Fig. 7 that the frictional entropy generation rate changes with the application of the magnetic field and with the increase in its gradient. With increasing magnetic field strength, the frictional entropy generated rate in the vicinity of the walls increases, and in the central part of the tube, less quantities are generated for entropy. The reason for

Fig. 2 Mesh configurations for the current simulation

Table 1 Checking the independence of the mesh

Mesh number in longitudinal direction	Mesh number in radial direction	Average convective heat transfer coefficient/W/m^{2}K	Error for h/%
300	20	602.14	8.5
350	25	640.85	2.7
400	30	658.76	0
450	35	660.31	0.2

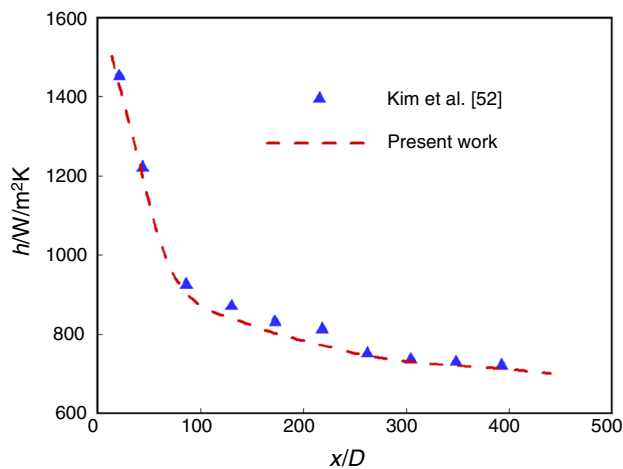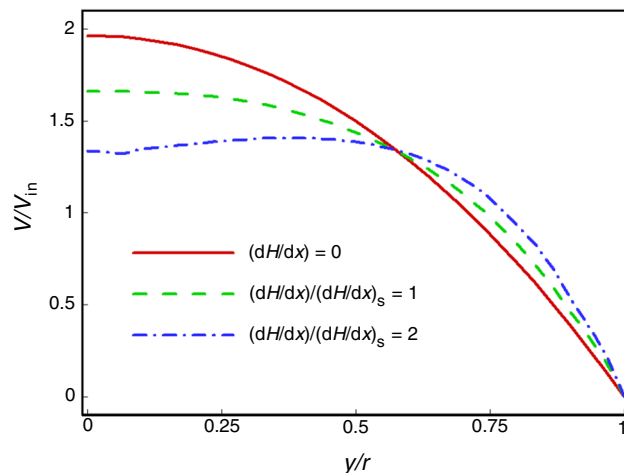**Fig. 3** Comparison between this paper with Kim et al. [52]

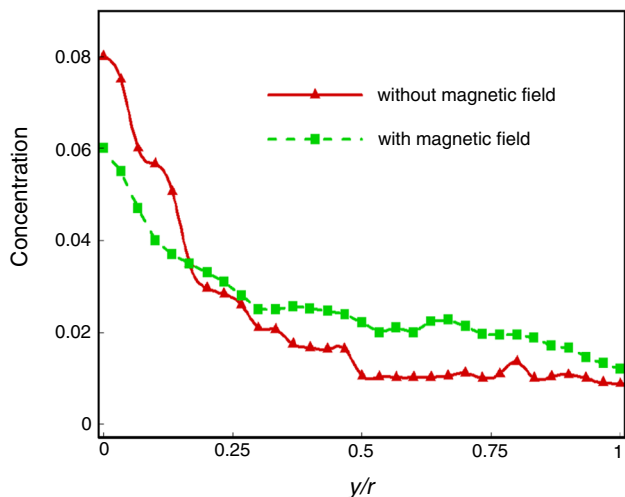**Fig. 5** Velocity profile at a cross section for different magnetic fields

Fig. 4 Distribution of nanoparticles concentration at a cross section

Fig. 6 Velocity profile at a cross section for $\phi = 0.01$, 0.03 and 0.05

these changes is due to the velocity changes described in Fig. 5. Figure 8 shows the contour of the frictional entropy generation rate near the inlet of the tube. It is found that more quantities are generated for frictional entropy in the vicinity of the wall in comparison with the other regions.

The dimensionless temperature (T_w/T_{in}) and local convective heat transfer coefficient on the tube wall for various gradients of the magnetic field are shown in Fig. 9 (ϕ
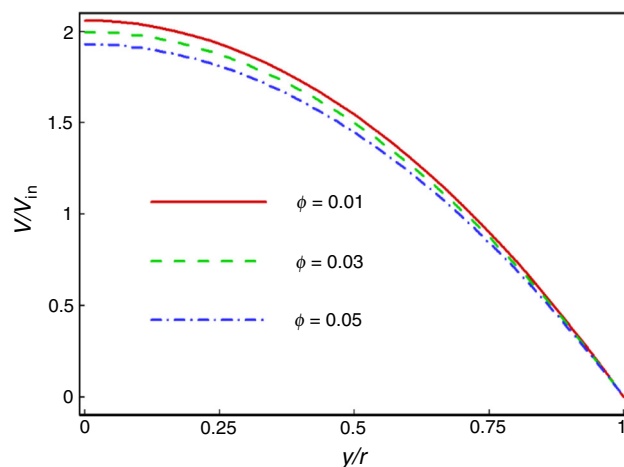
= 0.03, Re = 500). Figure 9a shows that with the application of the magnetic field, the convective heat transfer coefficient increases. The increase in convective heat transfer coefficient is due to the fact that the use of the magnetic field leads to an increase in speed near the wall of the tube (see Fig. 5). Also, it is found that the increase in magnetic field strength can also lead to an increase in the convective heat transfer coefficient (see Fig. 9a). Applying a magnetic field with a gradient of $(dH/dx)/(dH/dx)_s = 2$
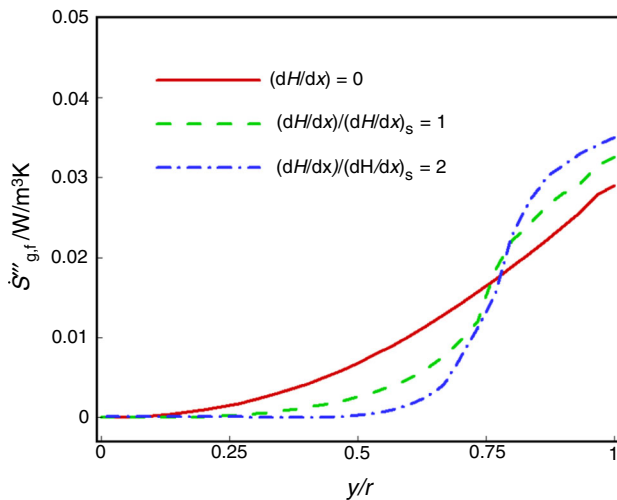
Fig. 7 Frictional entropy generation rate at a cross section for different magnetic fields
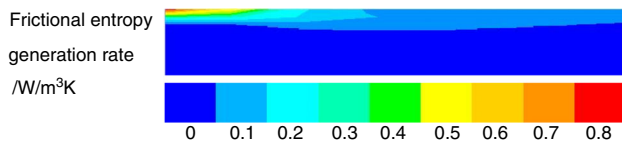

Fig. 8 Frictional entropy generation rate distribution near the inlet

can increase the local convective heat transfer coefficient up to 48 percent at $X = 0.3$. Moreover, it is clear that in the longitudinal direction of the tube, as the amount of magnetic field decreases, the convective heat transfer coefficient decreases, and then after $X = 0.61$, convective heat transfer coefficient values are equal to all the gradients. (After leaving the nanofluid flow from the magnetic field, its behavior resembles a state in which the magnetic field is not applied.) Moreover, in Fig. 9b it is clearly shown that the wall temperature of the tube decreases in part where the magnetic field is employed, and the more the magnetic field is increased, the better the tube surface cooling is done.
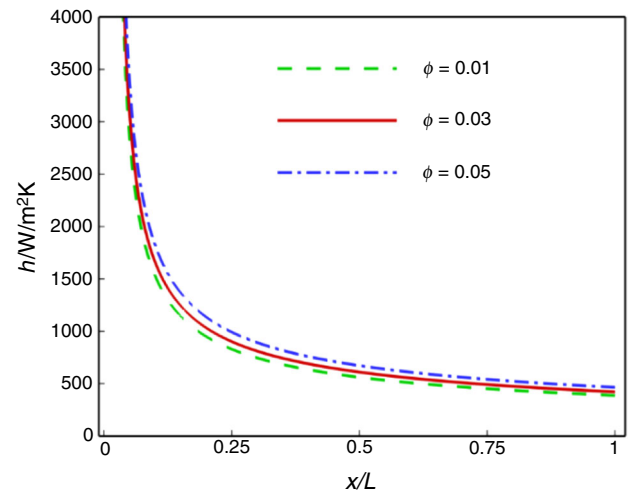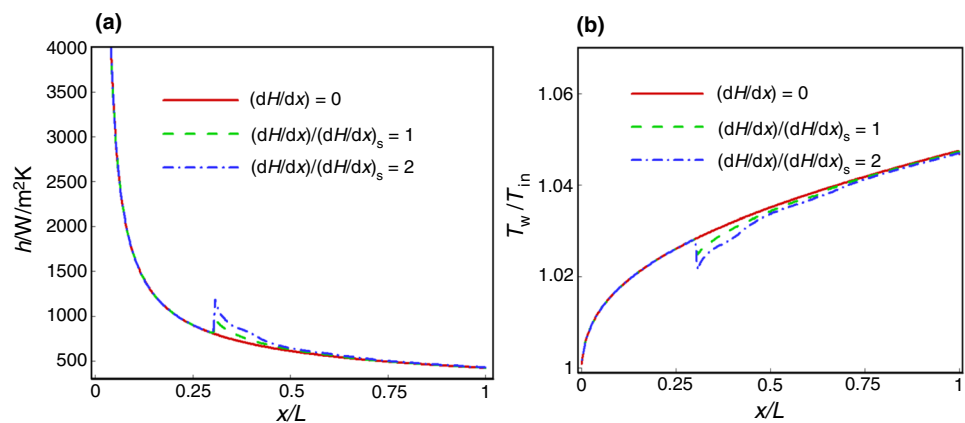

Fig. 10 Local convective heat transfer coefficient for three concentrations

The local convective heat transfer coefficient in a non-magnetized state for different concentrations is presented in Fig. 10 ($Re = 500$). It is clear from the figure that the use of nanoparticles and the addition of nanoparticles concentration lead to an increase in the convective heat transfer coefficient throughout the tube. As mentioned in previous papers, the reason for the increase is that the thermal conductivity of the nanofluid is increased by adding nanoparticles.

The convective heat transfer coefficient along the tube for the three different Reynolds number is shown in Fig. 11 ($\phi = 0.03$ and $(\mathrm{d}H/\mathrm{d}x)/(\mathrm{d}H/\mathrm{d}x)_s = 2$). The previous papers have been mentioned that the convective heat transfer coefficient is affected by the change in Reynolds number and increases as it rises throughout the tube. (The increase in the convective heat transfer coefficient in the first part of the tube is more evident.) By the increase in the Reynolds number, the wall temperature across the tube and the bulk temperature of the flow decreases, which ultimately leads to an increase in convective heat transfer
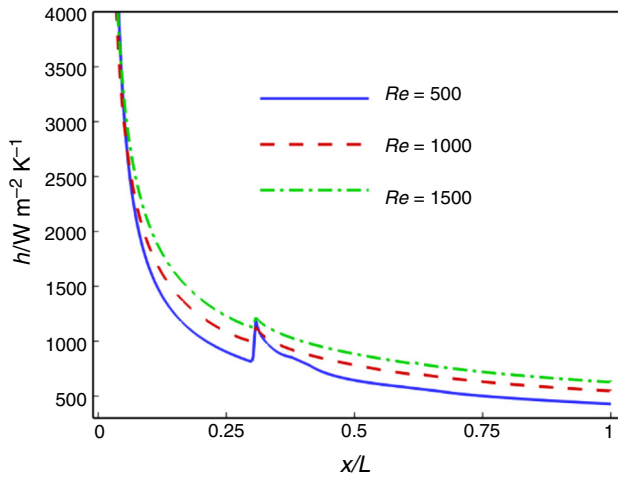
Fig. 9 a Local convective heat transfer coefficient and **b** non-dimensional temperature on the tube wall

Fig. 11 Local convective heat transfer coefficient for three Reynolds numbers
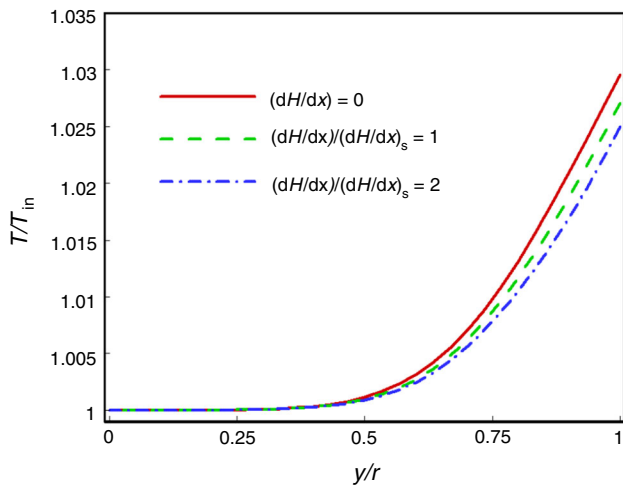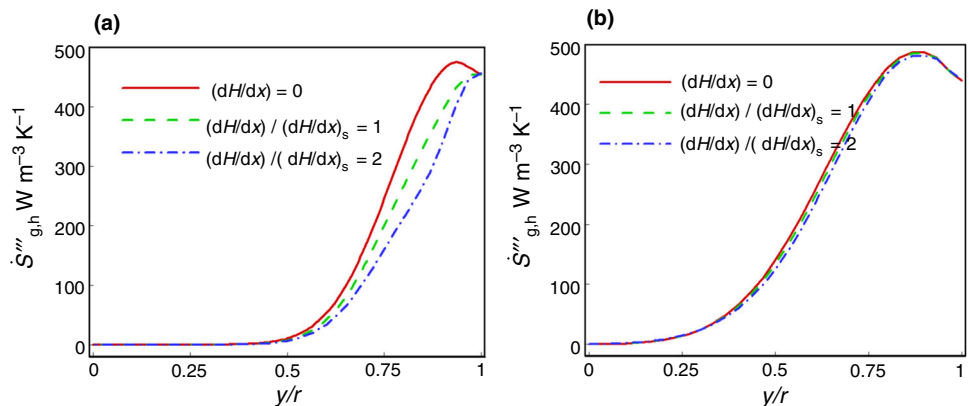

Fig. 12 Temperature profile at a cross section for different magnetic fields

coefficient according to Eq. 27. It is also clear from this figure that, as in Fig. 9a, the magnetic field also affects the

convective heat transfer coefficient and leads to increase, but with the difference that in the higher Reynolds number, the influence of the magnetic field decreases. Because, by decreasing Reynolds number, the effect of magnetic force becomes more important than the inertia force.

Figure 12 shows the temperature profile for a cross section of tube at $\phi = 0.03$, $Re = 500$ and for different magnetic fields with negative gradient. The temperature of nanofluid in the vicinity of the wall of the tube decreases with the application of the magnetic field. The reason is that by applying the magnetic field, the amount of velocity in the vicinity of the wall increases. But the temperature of the central parts of the tube does not affect the application of the magnetic field and increase its gradient. While the flow velocity in the central section of the tube decreases with the application of the magnetic field, and this cross section is close to the tube inlet, the growth of the thermal boundary layer does not cross over this cross section. Therefore, the effect of the magnetic field is not affected.

Figure 13 shows the thermal entropy generation rate in two different cross sections ($X = 0.33$ and near the outlet) for $\phi = 0.03$ and $Re = 500$. In this figure, the thermal entropy generation rate in the vicinity of the wall and in the central section of the tube is higher and lower, respectively. Because it is near the wall of the tube, there is a high temperature gradient; hence, in accordance with Eq. 22, more entropy is also generated. On the other hand, the thermal boundary layer of the nanofluid flow up to the tube outlet grows greatly, so the gradient of temperature is significant, which ultimately results in the higher thermal entropy at the outlet than the inlet proximity. It can be seen from this figure that, in the very near areas of the wall, the amount of thermal entropy generation rate decreases. (The decrease in the thermal entropy generation rate is more evident in Fig. 13b.) Because the heat flux is employed and the temperature increases along the wall and the temperature is in the denominator of Eq. 22, thermal entropy generation rate is reduced. In addition, it can be found that
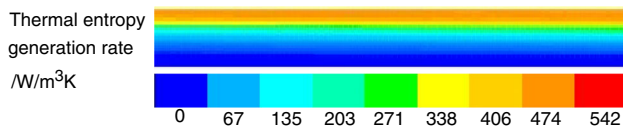
Fig. 13 Thermal entropy generation rate at: **a** $X = 0.33$ and **b** near the outlet

Thermal entropy
generation rate
/W/m^{3}K

0	67	135	203	271	338	406	474	542

Fig. 14 Contour of thermal entropy generation rate near the outlet

by applying the magnetic field, the thermal entropy generation rate changes. In Fig. 12, it is found that the magnetic field leads to decrease in the gradient of temperature in the vicinity of the wall, but the central parts of the magnetic field did not get any effect. Therefore, the thermal entropy generation rate in the vicinity of the wall is reduced by applying the magnetic field and increasing its strength. It is noteworthy that in Fig. 13a the nanofluid flow has received a greater influence on the magnetic field. Figure 14 shows the thermal entropy generation rate contour. It is seen that the highest and lowest thermal entropy generation rates occur, respectively, near the wall and in the central part of the tube. This is because the highest temperature gradients occur in the wall vicinity.

Figure 15 shows global non-dimensional values for the thermal and frictional entropy generation rate at three different magnetic field strengths ($\phi = 0.03$ and $Re = 500$). Here the subscript s refers to the non-magnetized state and $\phi = 0.03$. From Fig. 15a, it can be found that with the increase in the strength of the magnetic field, the global frictional entropy generation rate increases. As can be seen in Fig. 7, the frictional entropy generation rate in the vicinity of the wall and the central section of the tube increases and decreases with the application of the magnetic field, respectively, which ultimately leads to increase in global frictional entropy generation rates. From Fig. 15b, it can be found that the global thermal entropy generation rate decreases with increasing magnetic field strength, because the magnetic field reduces the thermal entropy generation rate (see Fig. 13).

The Bejan number contour is drawn (Fig. 16) near the tube outlet and inlet for $\phi = 0.03$ and $Re = 500$. It is clear from Fig. 16a that the Bejan number is much larger near
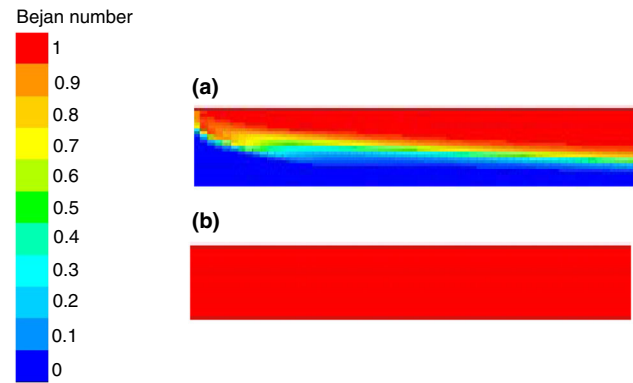
Bejan number

1	
0.9	
0.8	
0.7	
0.6	
0.5	
0.4	
0.3	
0.2	
0.1	
0	

Fig. 16 Bejan number contour: **a** near the inlet, **b** near the outlet

the vicinity of tube wall than the central part. As can be seen in Fig. 13, the high quantities of thermal entropy generation rate are occurred near the tube wall. This figure also shows that the nanofluid flow with movement in the tube leads to the high values of the Bejan number to the central part of the tube. In fact, hydrodynamic boundary layer growth is faster with respect to the thermal boundary layer. (For the nanofluid flow, Prandtl number is great.) Therefore, near the tube inlet, the boundary layer of the hydrodynamic develops quickly, while the boundary layer of the thermal develops in a region more distant from the tube inlet. In addition, Fig. 16b shows that the Bejan number is approximately 1 near the outlet. In fact, in this part, because of the thermal boundary layer growth, large amounts of thermal entropy are generated, which is a high value for the Bejan number indicating the predominance of thermal entropy generation rate.

The pressure drop at various magnetic field gradients is presented in Fig. 17 ($\phi = 0.03$ and $Re = 500$). From this figure, it can be found that for a negative gradient, if the magnetic field is used, the pressure drops increases, and this figure also shows that the pressure drop is exacerbated by increasing the strength of the magnetic field gradient, because in the negative gradient, the magnetic force enters Fe$_3$O$_4$ nanoparticles in the opposite direction.

Fig. 15 Integrated rates of: **a** frictional and **b** thermal entropy generation rates
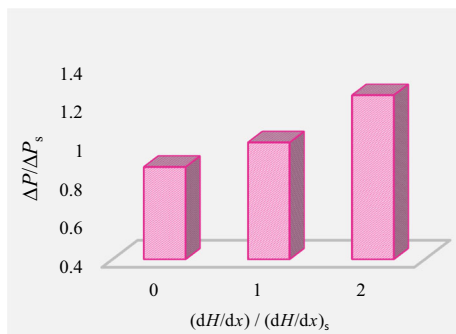
(a)

(b)
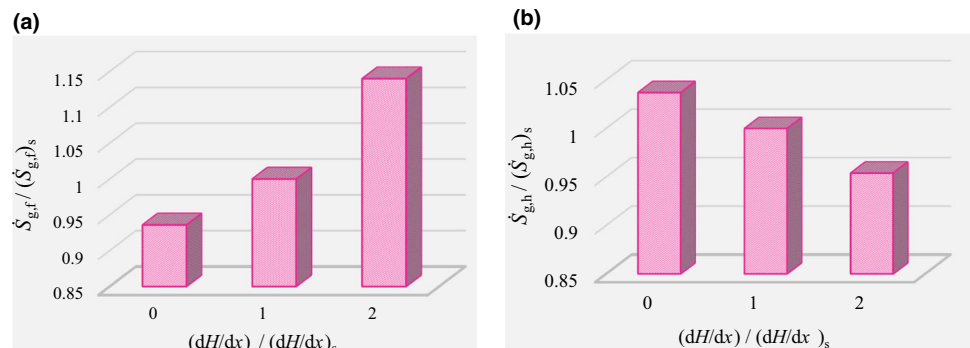
Fig. 17 Non-dimensionless pressure drop for different magnetic fields

Conclusions

The magnetic nanofluid flow containing Fe_3O_4 nanoparticles is simulated by the Euler–Lagrange model. The non-uniform magnetic field is applied on a part of tube; and the constant heat flux is applied on the tube wall. In this research, entropy generation rate (locally and globally), pressure drop, convective heat transfer coefficient, and distribution of nanoparticles concentration are studied. Results show that the highest and lowest thermal entropy generation rates occur, respectively, near the wall and in the central part of the tube. The convective heat transfer coefficient enhances by increasing Reynolds number and concentration. The nanofluid flow at the concentration of 0.05 possesses a profile of flatter velocity in comparison with concentration of 0.01. Also, the current simulation shows that by applying magnetic field:

- The velocity of the nanofluid in the tube central part and near the wall decreases and increases, respectively.
- In the vicinity of the wall and in the central part of the tube, the frictional entropy generation rate increases and decreases, respectively.
- In the vicinity of the wall, the thermal entropy generation rate reduces.
- The global thermal entropy generation rate decreases.
- The global frictional entropy generation rate enhances.
- The convective heat transfer coefficient increases.
- The wall temperature of the tube decreases in the part where the magnetic field is applied.
- The pressure drop along the tube increases.
- The temperature of the nanofluid in the vicinity of the wall decreases.

References

1. Mashayekhi R, Khodabandeh E, Akbari OA, Toghraie D, Bahiraei M, Gholami M. CFD analysis of thermal and hydrodynamic characteristics of hybrid nanofluid in a new designed sinusoidal double-layered microchannel heat sink. J Therm Anal Calorim. 2018;134:2305–15.
2. Rashidi S, Mahian O, Mohseni Languri E. Applications of nanofluids in condensing and evaporating systems. J. Therm Anal Calorim. 2018;131:2027–39.
3. Ahmadi AA, Khodabandeh E, Moghadasi H, Malekian N, Akbari OA, Bahiraei M. Numerical study of flow and heat transfer of water-Al2O3 nanofluid inside a channel with an inner cylinder using Eulerian-Lagrangian approach. J Therm Anal Calorim. 2018;132:651–65.
4. Mahian O, Kolsi L, Amani M, Estellé P, Ahmadi G, Kleinstreuer C, Marshall JS, Siavashi M, Taylor RA, Niazmand H, Wongwises S, Hayat T, Kolanjiyil A, Kasaeian A, Pop I. Recent advances in modeling and simulation of nanofluid flows-Part I: fundamentals and theory. Phys Rep. 2019;790:1–48.
5. Amani M, Amani P, Mahian O, Estellé P. Multi-objective optimization of thermophysical properties of eco-friendly organic nanofluids. J Clean Prod. 2017;166:350–9.
6. Zeibi Shirejini S, Rashidi S, Esfahani JA. Recovery of drop in heat transfer rate for a rotating system by nanofluids. J Mol Liquids. 2016;220:961–9.
7. Parizad Laein R, Rashidi S, Abolfazli Esfahani J. Experimental investigation of nanofluid free convection over the vertical and horizontal flat plates with uniform heat flux by PIV. Adv Powder Technol. 2016;27:312–22.
8. Bovand M, Rashidi S, Abolfazli Esfahani J. Optimum interaction between magnetohydrodynamics and nanofluid for thermal and drag management. J Thermophys Heat Transf. 2016;31:218–29.
9. Rashidi S, Bovand M, Esfahani JA. Opposition of magnetohydrodynamic and AL_2O_3–water nanofluid flow around a vertex facing triangular obstacle. J Mol Liq. 2016;215:276–84.
10. Rashidi S, Aolfazli Esfahani J, Ellahi R. Convective heat transfer and particle motion in an obstructed duct with two side by side obstacles by means of DPM model. Appl Sci. 2017;7:431.
11. Rashidi S, Abolfazli Esfahani J, Maskaniyan M. Applications of magnetohydrodynamics in biological systems-a review on the numerical studies. J Magn Magn Mater. 2017;439:358–72.
12. Rezaei Gorjaei A, Shahidian A. Heat transfer enhancement in a curved tube by using twisted tape insert and turbulent nanofluid flow. J Therm Anal Calorim. 2019;137:1059–68.
13. Bhattad A, Sarkar J, Ghosh P. Energetic and exergetic performances of plate heat exchanger using brine-based hybrid nanofluid for milk chilling application. Heat Transf Eng. 2019. https://doi.org/10.1080/01457632.2018.1546770.
14. Mahian O, Kolsi L, Amani M, Estellé P, Ahmadi G, Kleinstreuer C, Marshall JS, Taylor RA, Abu-Nada E, Rashidi S, Niazmand H, Wongwises S, Hayat T, Kasaeian A, Pop I. Recent advances in modeling and simulation of nanofluid flows—Part II: applications. Phys Rep. 2019;791:1–59.
15. de Castilho CJB, Fuller ME, Sane A, Liu JTC. Nanofluid flow and heat transfer in boundary layers: the influence of concentration diffusion on heat transfer enhancement. J Heat Transf Eng. 2019;40:725–37.
16. Gunnasegaran P, Zulkifly Abdullah M, Zamri Yusoff M, Kanna R. Heat transfer in a loop heat pipe using diamond-H_2O nanofluid. Heat Transf Eng. 2018;39:1117–31.
17. Zeinali Heris S, Edalati Z, Hossein Noie S, Mahian O. Experimental investigation of Al_2O_3/water nanofluid through equilateral triangular duct with constant wall heat flux in laminar flow. Heat Transf Eng. 2014;35:1173–82.
18. Sadeghinezhad E, Mehrali M, Akhiani AR, Tahan Latibari S, Dolatshahi-Pirouz A, Metselaar HSC, Mehrali M. Experimental study on heat transfer augmentation of graphene based ferrofluids in presence of magnetic field. Appl Therm Eng. 2017;114:415–27.

19. Sheikhnejad Y, Hosseini R, Saffar-avval M. Laminar forced convection of ferrofluid in a horizontal tube partially field with porous media in the presence of magnetic field. J Porous Media. 2015;18(4):437–48.

20. Azizian R, Doroodchi E, McKrell T, Buongiorno J, Hu LW, Moghtaderi B. Effect of magnetic field on laminar convective heat transfer of magnetite nanofluids. Int J Heat Mass Transf. 2014;68:94–109.

21. Amani M, Amani P, Kasaeian A, Mahian O, Wongwises S. Thermal conductivity measurement of spinel-type ferrite MnFe$_2$O$_4$ nanofluids in the presence of a uniform magnetic field. J Mol Liq. 2017;230:121–8.

22. Akar S, Rashidi S, Esfahani JA, Karimi N. Targeting a channel coating by using magnetic field and magnetic nanofluids. J Therm Anal Calorim. 2019;137(2):381–8.

23. Amani M, Amani P, Kasaeian A, Mahian O, Pop I, Wongwises S. Modeling and optimization of thermal conductivity and viscosity of MnFe$_2$O$_4$ nanofluid under magnetic field using an ANN. Scientific reports. 2017;7:17369.

24. Esmaeili E, Ghazanfar Chaydareh R, Rounaghi SA. The influence of the alternating magnetic field on the convective heat transfer properties of Fe$_3$O$_4$-containing nanofluids through the Neel and Brownian mechanisms. Appl Therm Eng. 2017;110:1212–9.

25. Bahiraei M, Hangi M. Investigating the efficacy of magnetic nanofluid as a coolant in double-pipe heat exchanger in the presence of magnetic field. Energy Convers Manage. 2013;76:1125–33.

26. Sheikhnejad Y, Hosseini R, Saffar Avval M. Experimental study on heat transfer enhancement of laminar ferrofluid flow in horizontal tube partially filled porous media under fixed parallel magnet bars. J Magn Magn Mater. 2017;424:16–25.

27. Yarahmadi M, Moazami Goudarzi H, Shafii MB. Experimental investigation into laminar forced convective heat transfer of ferrofluids under constant and oscillating magnetic field with different magnetic field arrangements and oscillation modes. Exp Therm Fluid Sci. 2015;68:601–11.

28. Bovand M, Rashidi S, Ahmadi G, Abolfazli Esfahani J. Effects of trap and reflect particle boundary conditions on particle transport and convective heat transfer for duct flow—A two-way coupling of Eulerian-Lagrangian model. Appl Therm Eng. 2016;108:368–77.

29. Rashidi S, Bovand M, Abolfazli Esfahani J, Ahmadi G. Discrete particle model for convective AL$_2$O$_3$–water nanofluid around a triangular obstacle. Appl Therm Eng. 2016;100:39–54.

30. Amani M, Amani P, Kasaeian A, Mahian O, Yan WM. Two-phase mixture model for nanofluid turbulent flow and heat transfer: effect of heterogeneous distribution of nanoparticles. Chem Eng Sci. 2017;167:135–44.

31. Maskaniyan M, Rashidi S, Abolfazli Esfahani J. A two-way couple of Eulerian-Lagrangian model for particle transport with different sizes in an obstructed channel. Powder Technol. 2017;312:260–9.

32. Fersadou B, Kahalerras h, Nessab W, Hammoudi D. Effect of magnetohydrodynamics on heat transfer intensification and entropy generation of nanofluid flow inside two interacting open rectangular cavities. J Therm Anal Calorim. 1–20.

33. Selimefendigil F, Oztop HF, Chamkha AJ. Analysis of mixed convection and entropy generation of nanofluid filled triangular enclosure with a flexible sidewall under the influence of a rotating cylinder. J Therm Anal Calorim. 2019;135:911–23.

34. Bahiraei M, Alighardashi M. Investigating non-Newtonian nanofluid flow in a narrow annulus based on second law of thermodynamics. J Mol Liq. 2016;219:117–27.

35. Shamsabadi H, Rashidi S, Abolfazli Esfahani J. Entropy generation analysis for nanofluid flow inside a duct equipped with porous baffles. J Therm Anal Calorim. 2019;135:1009–19.

36. Bahiraei M, Rezaei Gorjaei A, Shahidian A. Investigating heat transfer and entropy generation for mixed convection of CuO–water nanofluid in an inclined annulus. J Mol Liquids. 2017;248:36–47.

37. Akbarzadeh M, Rashidi S, Karimi N, Omar N. First and second laws of thermodynamics analysis of nanofluid flow inside a heat exchanger duct with wavy walls and a porous insert. J Therm Anal Calorim. 2019;135:177–94.

38. Mahian O, Mahmud Sh, Zeinaliheris S. Analysis of entropy generation between co-rotating cylinders using nanofluids. Energy. 2012;44:438–46.

39. Mahmud Sh, Fraser RA. Second law analysis of forced convection in a circular duct for non-Newtonian fluids. Energy. 2006;31:2226–44.

40. Bahiraei M, Jamshidmofid M, Amani M, Barzegarian R. Investigating exergy destruction and entropy generation for flow of a new nanofluid containing graphene–silver nanocomposite in a micro heat exchanger considering viscous dissipation. Powder Technol. 2018;336:298–310.

41. Shahsavar A, Ansarian R, Bahiraei M. Effect of line dipole magnetic field on entropy generation of Mn-Zn ferrite ferrofluid flowing through a minichannel using two-phase mixture model. Powder Technol. 2018;340:370–9.

42. Rezaei Gorjaei A, Soltani M, Bahiraei M, Kashkooli FM. CFD simulation of nanofluid forced convection inside a three-dimensional annulus by two-phase mixture approach: heat transfer and entropy generation analyses. Int J Mech Sci. 2018;146–147:396–404.

43. Minkowycz WJ, Sparrow EM, Murthy JY. Handbook of numerical heat transfer. Hoboken: Wiley; 2006. p. 697–724.

44. Aminfar H, Motallebzadeh R. Investigation of the velocity field and nanoparticle concentration distribution of nanofluid using Lagrangian-Eulerian approach. J Dispersion Sci Technol. 2012;33:155–63.

45. Ounis H, Ahmadi G, McLaughlin JB. Brownian diffusion of submicrometer particles in the viscous sublayer. J Colloid Interface Sci. 1991;143:266–77.

46. Saffman PG. The lift on a small sphere in a slow shear flow. J Fluid Mech. 1965;22:385–400.

47. Talbot L. Thermophoresis of particles in a heated boundary layer. J Fluid Mech. 1980;101:737–58.

48. Li A, Ahmadi G. Dispersion and deposition of spherical particles from point sources in a turbulent channel flow. Aerosol Sci Technol. 1992;16:209–26.

49. Zborowski M, Chalmers JJ. Magnetic cell separation. Amsterdam: Elsevier; 2008. p. 379–84.

50. Yamaguchi H. Engineering fluid mechanics. Netherlands: Springer; 2008. p. 497–542.

51. Ranz WE, Marshall WR. Evaporation from drops—Part I. Chem Eng Prog. 1952;48:141–6.

52. Kim D, Kwon Y, Cho Y, Li C, Cheong S, Hwang Y, Lee J, Hong D, Moon S. Convective heat transfer characteristics of nanofluids under laminar and turbulent flow conditions. Curr Appl Phys. 2009;9:119–23.

53. Bahiraei M, Hangi M. Studying flow and heat transfer characteristics of magnetic nanofluid under the effect of magnetic field using Euler- Lagrange approach. Int J Appl Electromagnet Mech. 2014;46:555–67.

54. Bahiraei M. A numerical study of heat transfer characteristics of CuO–water nanofluid by Euler-Lagrange approach. J Therm Anal Calorim. 2016;123:1591–9.

55. Mehryan SAM, Izadi M, Chamkha AJ, Sheremet MA. Natural convection and entropy generation of a ferrofluid in a square enclosure under the effect of a horizontal periodic magnetic field. J Mol Liq. 2018;263:510–25.

56. Mahalakshmi T, Nithyadevi N, Oztop HF, Abu-Hamdeh N. Natural convective heat transfer of Ag-water nanofluid flow inside enclosure with center heater and bottom heat source. Chin J Phys. 2018;56:1497–507.